Published in final edited form as:

Mitochondrion. 2016 September ; 30: 126–137. doi:10.1016/j.mito.2016.02.005.

Inactivation of Pif1 helicase causes a mitochondrial myopathy in mice

Sylvie Bannwarth[1,2], **Laetitia Berg-Alonso**[1], **Gaëlle Augé**[1,2], **Konstantina Fragaki**[1,2], **Jill E. Kolesar**[3], **Françoise Lespinasse**[1], **Sandra Lacas-Gervais**[4], **Fanny Burel-Vandenbos**[5], **Elodie Villa**[6], **Frances Belmonte**[3], **Jean-François Michiels**[5], **Jean-Ehrland Ricci**[6], **Romain Gherardi**[7], **Lea Harrington**[8], **Brett A. Kaufman**[3], and **Véronique Paquis-Flucklinger**[1,2]

[1]IRCAN, CNRS UMR 7284/INSERM U1081/UNS, Faculté de Médecine, Nice, France

[2]Service de Génétique Médicale, Hôpital Archet 2, CHU de Nice, Nice, France

[3]Department of Medicine, Center for Metabolism and Mitochondrial Medicine, University of Pittsburgh, Pittsburgh, USA

[4]Centre Commun de Microscopie Electronique Appliquée, Faculté des Sciences, Université de Nice Sophia Antipolis, Nice, France

[5]Service de Neuropathologie, Hôpital Pasteur, CHU de Nice, France

[6]INSERM U1065, Centre Méditerranéen de Médecine Moléculaire (C3M), équipe “contrôle métabolique des morts cellulaires”, Nice Sophia-Antipolis University, France

[7]INSERM U955, E10, Université Paris-Est, Créteil, France

[8]Université de Montréal, Institut de Recherche en Immunologie et en Cancérologie, 2950 chemin de Polytechnique, Montréal, Québec H3T 1J4, Canada

Abstract

Mutations in genes coding for mitochondrial helicases such as TWINKLE and DNA2 are involved in mitochondrial myopathies with mtDNA instability in both human and mouse. We show that inactivation of *Pif1*, a third member of the mitochondrial helicase family, causes a similar phenotype in mouse. *pif1*−/− animals develop a mitochondrial myopathy with respiratory chain deficiency. *Pif1* inactivation is responsible for a deficiency to repair oxidative stress-induced mtDNA damage in mouse embryonic fibroblasts that is improved by complementation with mitochondrial isoform *mPif1*^{67}. These results open new perspectives for the exploration of patients with mtDNA instability disorders.

Keywords

Pif1 helicase; mtDNA instability; mitochondrial myopathy; mitochondrial disease

Correspondence to: Prof. Véronique Paquis-Flucklinger, IRCAN UMR7284 / INSERM U1081 / UNS, School of Medicine, 28 av de Valombrose, 06107 Nice cedex 2, France. Tel: (33) 4 93 37 77 86, Fax: (33) 4 93 37 70 33, paquis@hermes.unice.fr.

1. INTRODUCTION

The PIF1 helicase family is a group of 5′->3′ directed, ATP dependent, super family 1B helicases found in nearly all eukaryotes. *Saccharomyces cerevisiae* (Sc) *PIF1* was first identified as a gene whose mutation results in reduced recombination between the mitochondrial DNA (mtDNA) of rho− and rho+ strains (Foury and Kolodynski, 1983). *ScPIF1* was rediscovered in a screen for mutations that affect telomeres (Lahaye et al., 1993). The nuclear Pif1p isoform is involved in numerous functions, including: inhibition of telomere addition to double strand breaks (DSBs), inhibition of telomerase with an enrichment of ScPif1p at telomere ends and a negative regulation of telomere length by removing telomerase from telomeres, participation in resolving G-quadruplex structures, and Okazaki fragment maturation (Bochman et al., 2010; Li et al., 2014; Wilson et al., 2013; Zhou et al., 2000). The mitochondrial PIF1 isoform plays an important role in mtDNA maintenance. *Scpif1* mutants lose their mtDNA, especially at high temperatures, and are defective in mtDNA repair. Pif1p binds to mtDNA and may prevent accumulation of oxidative DNA damage in mtDNA (de Souza-Pinto et al., 2010). Both mitochondrial and nuclear isoforms are expressed from the single *ScPIF1* open reading frame but use different translational start sites with a mitochondrial targeting signal (MTS) being located between the first and the second translational start site.

PIF1 is also found both in the nucleus and mitochondria of human cells (Futami et al., 2007; Kazak et al., 2013). The hPIF1 nuclear isoform inhibits telomerase, and the helicase domain of hPIF1 preferentially binds and unwinds DNA structures that mimic stalled replication forks (George et al., 2009; Zhang et al., 2006). Furthermore, PIF1 is a highly active evolutionarly conserved, G-quadruplex helicase (Paeschke et al., 2013; Sanders, 2010). As in human, mPIF1 is found only in proliferating cells and interacts with telomerase in mouse extracts, suggesting that mPIF1 would affect telomeres (Snow et al., 2007). However, the *pif1* knockout (KO) mice are viable, with no change in telomere length, even after several generations, and no gross chromosomal rearrangements (Snow et al., 2007). These results suggest that PIF1 telomere function could be redundant with that of other helicase in mice. Nevertheless, the mitochondrial functions of PIF1 in mouse and human are currently not characterized.

In this study, we examined the phenotype of *pif1*−/− mice in order to analyze the consequences of *PIF1* inactivation on mitochondrial functions. Knockout animals develop mitochondrial myopathy with respiratory chain deficiency and a low amount of mtDNA deletions after 1 year of age. Furthermore, we show that mPIF1 associates with mtDNA and increases recovery from oxidative damage. These findings strongly support a role for PIF1 in mtDNA maintenance *in vivo*.

2. MATERIAL AND METHODS

2.1 Generation of *Pif1−/−* mice

A targeting construct was designed to delete a region of mPIF1 that spanned the first five conserved helicase motifs of *mPif1* as described by Snow and colleagues (Snow et al.,

2007). Chimeric and founder mice were generated and the complete absence of the *mPif1* transcript was shown by Northern analysis of *mPif1* MEFs (Snow et al., 2007).

2.2 Histopathology and ultrastructure

Muscle samples were frozen in cooled isopentane and stored in liquid nitrogen for histological and histoenzymatic analysis including Gomori modified trichrome staining, cytochrome *c* oxydase (COX) activity, succinate dehydrogenase (SDH) activity and double COX/SDH staining, and nicotinamide adenine dinucleotide dehydrogenase tetrazolium reductase staining (NADH-TR) according to standard protocols. For transmission electron microscopy analysis, muscles and hearts were dissected and rapidly fixed in 2% glutaraldehyde in 0.1 M cacodylate buffer, rinsed in the same buffer, post-fixed for 1h in 1% osmium tetroxide and 1% potassium ferrocyanide in 0.1 M cacodylate buffer to enhance the staining of membranes. Tissues were rinsed in distilled water, dehydrated in acetone and embedded in epoxy resin. Contrasted ultrathin sections (70 nm) were analyzed under a JEOL 1400 transmission electron microscope mounted with a Morada Olympus CCD camera. At least three animals per group were analyzed.

2.3 Voluntary exercise

Hamster-sized metal cages wheels (diameter 24 cm) with digital magnetic counters (Intellibio) were placed into 37 X 20 X 16 cm cages to measure the voluntary daily running distance for 2 weeks. Six *pif1*−/− mice with six littermates at 14 months of age and six *pif1*−/− mice with six littermates at 3 months of age were tested (three males and three females in each group).

2.4 OXPHOS spectrophotometric measurements

Enzymatic spectrophotometric measurements of the OXPHOS respiratory chain complexes and citrate synthase were performed at 37°C on tissue homogenates according to standard procedures (Rustin et al., 1994). Proteins were measured according to Bradford microassay (Bradford, 1976) and results were expressed as nmol/min/mg of proteins normalized to citrate synthase activity.

2.5 Long extension PCR (LX-PCR) and Southern blot for detection of mtDNA deletions

LX-PCR were performed with Expand long template PCR system (Roche Applied Science). Reaction mixtures contained 200ng of template genomic DNA, 5µl Buffer 3, 1mM dXTP (Roche Applied Science), 200ng primers and 3.75Units of mix Taq Polymerase. Primers sequence are listed in supplementary table 1 (Edgar et al., 2009). The PCR program used for amplification of the 12.8kb mouse mtDNA fragment was: 95°C 5 min, followed by 20 cycles (10 sec at 95°C, 30 sec at 62°C, 13 min at 68°C), followed by 10 cycles (10 sec at 95°C, 30 sec at 62°C, 13 min + 20 sec per cycle at 68°C), with a final extension of 5 min at 68°C. PCR products were loaded on a 0.8% agarose gel and migrated 7h at 130Volts. Southern blots were performed as previously described (Tyynismaa et al., 2004). 5µg of genomic DNA were digested with *Afe*I endonuclease, electrophoresed on 0.8% agarose gel and transferred to Hybond N+ membrane (Roche Applied Science). Blots were hybridized with a probe obtained by PCR amplification of mouse mtDNA (primers spanning positions

15809–15810, supplementary table 1) and labelled using digoxigenin random priming method (Roche Applied Science).

2.6 mtDNA quantification

The mouse mtDNA content was determined by real-time PCR using TaqMan probes, specific for mitochondrial 12S rRNA. Nuclear gene used for normalization was mouse *GAPDH*. Mitochondrial 12S rRNA and nuclear *GAPDH* genes were individually amplified by real-time PCR using primers m12S-F/m12S-R and those from mouse *GAPDH* gene expression assay kit (Applied Biosystems) with corresponding TaqMan probes (Supplementary table 1). The real-time PCR reaction was performed 3 times, in duplicate for each reaction. PCR reaction mixture (20μl) contained 20ng of genomic DNA, 1X LightCycler 480 probes master mix (Roche Applied Science), 1μl of *GAPDH* gene expression assay kit (Life Technologies) or 0.3 nM of each primer and 6 μM of each probe. The PCR amplification, performed in the Light Cycler LC480 apparatus, consisted of a single denaturation-enzyme activation step for 10 min at 95°C, followed by 45 amplification cycles of 15 sec at 95°C, 40 sec at 60°C. A single acquisition was done at the end of each annealing step, and data were analyzed using LightCycler software version 1.5.0.39 (Roche Applied Science). The *ratio* of mtDNA amplicon to nuclear DNA amplicon was used as a measure of mtDNA content in each specimen.

2.7 Somatic mtDNA mutations

Total DNA was extracted from the muscles and heart of three *pif1*−/− mice with three littermates at 14 months of age and of three *pif1*−/− mice with three littermates at 3 months of age. The somatic mtDNA mutation load was determined by targeted next-generation sequencing (NGS) with Ion PGM System (Ion Torrent). Whole mtDNA was amplified from 80ng of genomic DNA, using the Roche Expand Long Template Kit (Roche Applied Science), in one LX-PCR amplicon, as previously described. Primers sequence are listed in supplementary table 1 (Edgar et al., 2009). Library preparations were performed following the manufacturer's instructions (Ion Xpress plus Fragment Library kit, Life Technologies) for 200bp single-end reads. Emulsion PCR was performed on pooled librairies (Ion One Touch 200 Template Kit v2; Life Technologies). Samples were prepared according to the instructions provided with Ion PGM 200 Sequencing Kit (Life Technologies) protocol. Six pooled samples were loaded on an Ion 314 chip.

2.8 RNA isolation and Quantitative Real-Time PCR

Total RNA from tissues was extracted using TRIzol reagent (Life Technologies) and purified with PureLink RNA kit (Life Technologies). Prior to reverse transcription, residual genomic DNA was removed from total RNA with DNase I (Life Technologies). cDNA was then reverse-transcribed using transcription first strand cDNA synthesis kit (Roche Applied Science) with 1μg total RNA and oligo-dT as primer. All PCR were performed in triplicate. Quantitative RT-PCR was carried out using SYBR Green master mix (Roche Applied Science) on a Light Cycler LC480. Results were normalized to *OAZ1* or *HPRT*. Primer sequences are shown in supplementary table 1.

2.9 Plasmid construction

Coding sequence of the mitochondrial PIF1 isoform (mPIF1^{67}) was cloned into pBABE after amplification by PCR and enzyme-mediated recombination according to the manufacturer (Life Technologies). To generate pEGFP-N1-*mPif1*^{67} (mPIF1^{67}-EGFP) construct, the ORF was amplified by PCR from the pBABE plasmid with primers containing terminal restriction sites (Kazak et al., 2013). The resulting PCR product was digested and ligated into the *Xho*I-*Age*I sites of pEGFP-N1. Primers used are listed in supplementary table 1. Constructs were verified by sequencing.

2.10 Cell culture

HeLa cells were maintained in Dulbecco-modified Eagle medium (DMEM) (GE Healthcare) supplemented with penicillin (100U/ml)/streptomycin (0.1mg/ml), 10% fetal calf serum (FCS) (GE Healthcare), at 37°C in a humidified atmosphere with 5% CO_2 in air. For transient transfections, cells were seeded onto 100-mm-diameter culture sterile dishes. At 60–80% confluence, cells were transfected using a standard calcium-phosphate procedure as previously described (Neyton et al., 2004). After a 24h-period, transfected cells were harvested for mtDIP-PCR, western blot or confocal microscopy analyses.

Primary mouse embryonic fibroblasts (MEFs) were prepared by mincing 14.5-day-old embryos of C57Bl/6J or *pif1*−/− mice, treating them with trypsin, and plating in DMEM supplemented with 10% FCS. Cells were maintained in DMEM supplemented with penicillin (100U/ml)/streptomycin (0.1mg/ml), 10% FCS, at 37°C in a humidified atmosphere with 5% CO_2 in air.

2.11 Immortalization of primary MEFs

pif1+/+ and *pif1*−/− primary MEF cells were plated in 100-mm dishes in DMEM, 10% fetal bovine serum/fetal calf serum (FBS/FCS) and allowed to grow to approximately 70% confluence. Cell lines PA317 hTERT and PA317 E7/TEL were each plated in 100-mm dishes and allowed to grow to confluence in DMEM, 10% FBS/FCS (Morales et al., 1999). On the day of immortalization, virus-containing medium from each plate was filtered through a 0.45 μm filter, combined and 4 μg/mL polybrene added. MEFs were washed once with PBS, and immortalized by adding virus-containing medium with polybrene followed by overnight incubation. After 16 hours, cells were washed once with PBS and fresh medium added (no virus). Cells were passaged alongside non-immortalized MEFs and compared for senescence. Only immortalized cells grew beyond three serial passages.

2.12 Transduction of immortalized primary *pif1* +/+ and *pif1*−/− MEFs

Packaging cells were plated into three separate 100-mm dishes and allowed to grow to approximately 70% confluence. On day 1, Turbofect (Thermo Scientific) and serum-free medium were used according to manufacturers' directions to transiently transfect one plate each with 3 μg vector DNA containing pBABE-puro or pBABE-*mPIF1*^{67}. Cells were incubated overnight and medium changed on day 2. On day 3, virus-containing medium from plate dishes was filtered through a 0.45 μm filter and 4 μg/mL polybrene added. Primary MEF target cells (40% confluent) were washed once with PBS, and viral supernatant with polybrene added and incubated overnight. Medium was changed on day 4,

and on day 5, fresh medium with 2 μg/mL puromycin (Sigma-Aldrich) added. Cells were passaged as necessary under puromycin selection to establish the cell lines for subsequent experiments.

2.13 Isolation of mitochondria and western blot analysis

Mitochondria were isolated from HeLa cells using Q-Proteome mitochondria isolation kit (Qiagen) as described by the manufacturer. Proteinase K treatment was performed as previously described (Bannwarth et al., 2012). SDS-Polyacrylamide gel electrophoresis (PAGE) and immunoblotting were performed using standard protocols. Samples were immunoblotted with mouse monoclonal anti-GFP (Santa Cruz Biotechnology), mouse monoclonal anti-MFN2 (outer mitochondrial membrane protein, Abcam), and rabbit polyclonal anti-SMAC (mitochondrial intermembrane space protein, Abcam). The cytosolic rabbit polyclonal anti-GAPDH (Abcam), and nuclear mouse monoclonal anti-PCNA (BD Biosciences) antibodies were also used to ensure the absence of contamination by cytosolic or nuclear proteins. Signals were detected using a Chemiluminiscence system (Immobilon western chemiluminescent HRP substrate, Millipore).

2.14 Confocal microscopic analysis

HeLa cells were grown and transfected by calcium phosphate precipitation on glass coverslips. For mitochondrial staining, cells were incubated in a 100nM solution of MitoTracker red (Life Technologies) for 15 min, replaced by HeLa cells culture medium for 2h at 37°C, and washed in PBS. The samples were fixed with paraformaldehyde 15 min, washed with PBS, mounted on glass slides using 12% Mowiol (Calbiochem), and analyzed using a Zeiss LSM510 meta confocal laser-scanning microscope.

2.15 mtDIP-PCR assay of PIF1-mtDNA interaction

The mtDIP method is based on the principle of chromatin immunoprecipitation (ChIP) assay and was exactly performed as previously described (Bannwarth et al., 2012).

2.16 Treatment of cells with H_2O_2 or MMS

Immortalized MEFs were plated in triplicate in 100mm-diameter culture sterile dishes at 60–70% confluence 20h before treatment. H_2O_2 (30%, Sigma-Aldrich) or MMS (99%, Sigma-Aldrich) were diluted into PBS. The concentration of H_2O_2 was determined by absorbance at 260nm as described (Shull et al., 1991). Monolayer cultures were exposed to 150 μM H_2O_2 for 30 min at 37°C or to 2mM MMS for 45 min at 37°C in serum free medium that was replaced by complete medium culture and incubated for the indicated times. Before genomic DNA extraction, the medium culture was removed and plates were rapidly frozen in N_2 liquid and stored at −80°C. High molecular weight DNA from cell lines was isolated using a Qiagen genomic tip 20G kit (Qiagen) as described by the manufacturer.

2.17 mtDNA damage and repair assays

The qPCR assay measures the DNA lesions in a genomic segment of interest. DNA lesions, including H_2O_2- or MMS-induced damages, block the progression of the Taq DNA polymerase resulting in a decreased amplification of a target sequence (Furda et al., 2012;

Rouzier et al., 2012; Yakes and Van Houten, 1997). PCR quantification was normalized with a small target PCR which is not affected by H_2O_2 or MMS treatment and serves as an indicator of relative copy number and PCR quality of the genomic extract. Therefore, for each sample, 3 separates PCR reactions were performed with 3 different cycle numbers to determine quantitative conditions. A 10kb mouse mtDNA fragment was amplified in a Applied PCR System 2720 with Expand long template PCR system (Roche Applied Science). Primer sequences are listed in supplementary table 1. Reaction mixtures contained 200ng of template genomic DNA, 1X Buffer 3, 0.5mM deoxynucleotide triphosphate (Roche Applied Science), 200ng of each primer and 3.75Units of Taq Polymerase mix. A 117bp mouse mtDNA small fragment was amplified to determine the copy number of mitochondria, using 2.5Units of Taq DNA Polymerase (Roche Applied Science), 200ng of template genomic DNA, 1X Taq DNA Polymerase buffer, 0.2mM deoxynucleotide triphosphate (Roche Applied Science), and 200ng of each primer. PCR programs and Quant-iT PicoGreen method used for the quantification of PCR products were previously described (Bannwarth et al., 2012).

2.18 Reactive oxygen species (ROS) detection

CellROX green reagent (Life technologies) was added to cell culture medium at a concentration of 500 nM for 30 min at 37°C, 5% CO2, protected from light. The cells were then analyzed by flow cytometry using a MACS-Quant Analyzer (Miltenyi Biotec). As a positive control, cells were treated 30 min with tert-butyl hydroperoxide (TBHP) at 200 μM, and as a negative control cells were incubated with N-acetylcysteine (NAC) at 500 μM for 1 hour prior to treatment with 200 mM TBHP.

2.19 Circular: Linear mtDNA analysis

From frozen culture plates, cells were scraped in proteinase K digestion buffer and digested overnight as previously described (Kolesar et al., 2013). Samples were quantified and mtDNA resolved into relaxed circular and linear genomes by single dimension intact mtDNA agarose gel electrophoresis (1D-IMAGE) prior to quantitation (Kolesar et al., 2014).

3. RESULTS

3.1 *pif1−/−* mice show histological features of mitochondrial myopathy

Patients with mtDNA instability disorders often develop mitochondrial myopathy during adulthood with little functional consequences. We therefore first sacrified 14-month-old mice to analyze muscle histopathology and ultrastructure (Fig. 1A–L). *pif1*−/− animals presented an accumulation of mitochondria in the subsarcolemmal region of type 1 muscle fibers on Gomori trichrome stain (Fig. 1D). Although histological analysis found no COX negative (COX-) muscle fibers, moth-eaten fibers were observed with both COX and NADH-TR staining (Fig. 1E,F). Electron microscopy studies (Fig. 1G–L) confirmed muscle dysfunction and mitochondrial abnormalities by showing necrotic muscle fibers characterized by an erasing of the striation and a general disorganization of sarcomeres associated with a characteristic emphasis of mitochondria contours (Fig. 1H,K). Subsarcolemmal mitochondria accumulation, lipid droplets and abnormal mitochondria were also found in non-necrotic fibers including elongated or enlarged and swollen mitochondria

with altered cristae organization (Fig. 1I,L). In some fibers, the coexistence of a mitochondrial overload and necrotic alteration of myofilaments was also observed.

No signs of mitochondrial dysfunction were noted during the first months of life by optic microscopy analysis in mutant mice (not shown). However, mitochondria with altered morphology and myofibrillar disorganization were observed in a few number of muscle fibers by electron microscopy in *pif1*−/− animals from the age of 3 months (not shown).

We also examined the hearts of mice without finding abnormalities by light microscopy analysis. However, electron microscopy showed swollen mitochondria and disorganization of some cardiomyocytes in 14-month-old animals only (Supplementary Fig. 1). These data demonstrate progressive defects in the *pif1*−/− mice, with an overt mitochondrial requirement for PIF1 in skeletal muscle in adult mice.

3.2 The physical performance of *pif1*−/− mice is decreased

Because of the histological abnormalities found in the muscle of *pif1* KO mice, we studied the physical performance of mutant animals at one year of age. The distance run on voluntary running-wheel exercise has been shown to reflect the endurance capacity. As previously described, we observed that C57BL/6J female mice ran longer than male mice (Fig. 2) (De Bono et al., 2006). We found impairment of exercise capacity in *pif1*−/− mice with a daily running distance significantly lower compared to controls both in males ($p<0.05$) and females ($p<0.01$) (Fig. 2A). The distance per day (mean ± SD) was 1.7 ± 1.5 km in *pif1*−/− males *versus* 5.6 ± 1.1 km in control males and 2.4 ± 1.0 km in −/− females *versus* 7.0 ± 0.4 km in control females. In the younger three months aged mice, the difference between knockout and wild-type mice was smaller but still significant. The distance per day was 4.4 ± 0.7 km in *pif1*−/− males *versus* 6 ± 0.6 km in control males and 4.8 ± 0.9 km in −/− females *versus* 6.7 ± 0.6 km in control females (Fig. 2B).

At birth and during the first months of life, there was no difference in weight between KO and control mice in males or females. However, *pif1*−/− animals presented a significant gain of weight from the age of 6 months in males and 5 months in females (Fig. 2C). When we compared the body weight-normalized running distance (m/g), the exercise capacity was still significantly different between *pif1*−/− and control mice at one year of age ($p<0.05$): 3.8 fold less in males and 4.3 fold less in females (Fig. 2D).

3.3 Respiratory chain deficiency with low amount of mtDNA deletions in muscle of *pif1*−/− mice

Mitochondrial function was assessed by enzymatic spectrophotometric measurements of the individual respiratory chain complexes in muscle of KO mice, which presented characteristic histological changes at 14 months of age. We observed a significant decrease of complex I activity in both 14 month and 3 month-aged *pif1*−/− animals compared to controls (Fig. 3A, B). We also characterized respiratory chain function in the hearts of KO mice, which revealed a decrease of complex I and III activity, but only in old animals (Fig. 3C, D), which is consistent with the cardiac abnormalities found by electron microscopy.

Because loss of *PIF1* in yeast causes mtDNA deletions (Schulz and Zakian, 1994), we searched for mtDNA deletions in KO and age-matched control mice by long extension PCR (LX-PCR). Amplification of muscle mtDNA of *pif1*−/− animals at 14 months of age resulted in multiple products, corresponding to full-size mtDNA and molecules with deletions of multiple sizes (Fig. 4A). Only the 12.8kb product was amplified from control muscles. No deletion was found in other tissues tested except for one KO mouse that had one single deleted PCR product of around 3kb in brain, heart and kidney but not in liver (Fig. 4A). Cloning and sequencing of deletion breakpoints revealed that the 3kb amplicon contained a single 9676 bp deletion between nt 5597 and nt 15271. The deletions could not be seen on Southern blot except for the deleted population corresponding to the 3kb amplicon upon overexposure of autoradiography (Fig. 4B), suggesting that the amount of deleted molecules is very modest. Quantification of mtDNA copy number against the nuclear *GAPDH* gene revealed no depletion in any tissue examined (muscle, heart, brain, liver and kidney) neither in old (Fig. 4C) nor in young (not shown) *pif1*−/− mice.

Next-generation sequencing revealed that 3-month-old or 14-month-old *pif* KO animals did not have a detectable increase in somatic mtDNA point mutation load in their muscle and heart samples (not shown). In order to determine the putative role of endogenous ROS production in mtDNA mutagenesis, we quantified the level of ROS production in *Pif1*−/− cells. In basal condition, the endogenous ROS level was similar in control and *pif1*−/− MEFs suggesting that mutagenesis associated with endogenous ROS production is not increased in KO mice compared to control animals. Interestingly, treatment with tert-butylhydroperoxide (TBHP), an oxidative stress inducer, resulted in marked increase of ROS level in *pif1*−/− MEFs compared to control MEFs (Fig. 4D).

3.4 Mitochondrial deficiency in *pif1−/−* mice is not secondary to Pif1-dependent telomere dysfunction

A lot of human diseases (muscle atrophy, cardiovascular disorders, diabetes…) implicate mitochondrial deficiency and telomere dysfunction. Dysfunctional telomeres activate p53 which in turn binds and represses promoters of *Ppargc1α* (*PGC-1α*) and *Ppargc1β* (*PGC-1β*), two key regulators of mitochondrial physiology, leading to impaired mitochondrial function (Sahin et al., 2011). *pif1*−/− mice apparently did not show a telomere phenotype so we analyzed PGC pathway to verify that diminished mitochondrial function that we observed was not secondary to an undetected telomere dysfunction (Snow et al., 2007). Quantitative reverse transcriptase polymerase chain reaction analysis (RT-qPCR) of muscle and heart tissues from 14 month-old *pif1*−/− mice showed no decreased *PGC-1α* and *PGC-1β* expression and their critical targets such as *Sirt3*, *CD36* and *Acox1* genes (Fig. 5). Thus, respiratory chain defect and histological changes found in these tissues were likely secondary to the absence of a PIF1 mitochondrial isoform rather than a PIF1-dependent telomere dysfunction.

3.5 Mitochondrial localization of mPIF1 and physical association with mtDNA

It has been recently shown that generation of mitochondrial-targeted forms of human and mouse PIF1 occurs *via* downstream alternative translation initiation (dATI) (Kazak et al., 2013). In mouse, dATI occurs from the AUG encoding methionine 67 of PIF1 and the

generated mitochondrial isoform is cleaved after mitochondrial import. To confirm this result, we treated isolated mitochondria, from *mPIF1^{67}-EGFP* transfected HeLa cells, with proteinase K. As shown in Figure 6A, mPif1^{67}-EGFP was resistant to protease treatment indicating that the fusion protein is present inside mitochondria. We also observed a shorter protein (m), which was also resistant to degradation by proteinase K, presumably corresponding to the product of the mature mitochondrial isoform (Kazak et al., 2013). As expected, MFN2 (outer mitochondrial membrane) was digested by proteinase K while SMAC (intermembrane space protein) was resistant to protease digestion. Confocal microscopy analysis futher confirmed mitochondrial targeting of mPIF1^{67}-EGFP (Fig. 6B).

To test wether mPIF1^{67}-EGFP associated with mtDNA, we then performed the mtDNA immunoprecipitation assay (mtDIP assay) and PCR analysis (Bannwarth et al., 2012). Mitochondria were isolated from *mPIF1^{67}-EGFP* transfected HeLa cells and proteins that interact with mtDNA were chemically crosslinked. The samples were then submitted to immunoprecipitation with anti-GFP antibody, as well as negative control antibodies (anti-FLAG and non-specific IgG) (Fig. 6C). The precipitated DNA was isolated and analyzed by PCR for mtDNA, using pairs of primers specific for coding regions (amplicons C, E and G) (Fig. 6C). These primers do not allow any amplification from DNA extracted from Wall-2A-ρ^0 cells, demonstrating that the corresponding amplicons do not result from the amplification of nuclear pseudogenes (Bannwarth et al., 2005). DNA isolated prior immunoprecipitation from each sample was used as positive control (input) for the PCR reaction. As shown in Figure 6C, mtDNA sequences were amplified only in GFP-precipitated samples, and not in the negative control IgG and FLAG samples or untransfected cells. These results are consistent with the localization of Pif1 inside mitochondria and show that the mitochondrial isoform of this helicase associates with mtDNA.

3.6 *mPif1* inactivation affects mtDNA repair following DNA damage induced by oxidative stress that is improved by complementation with *mPif^{67}*

To assess the role of PIF1 in mtDNA damage, we determined whether this protein could influence mtDNA repair kinetics caused by oxidative stress. Lesions in mitochondrial genome due to H_2O_2 treatment were first assessed by qPCR-based assay in which base lesions, abasic sites or strand breaks interfere with the amplification of long DNA targets (Rouzier et al., 2012; Yakes and Van Houten, 1997). Long PCR products serve as sensitive probes for lesions introduced by oxidative stress, where shorter control amplicons are less likely to be damaged and serve to normalize the samples. We treated control and *pif1*−/− MEFs with 150μM H_2O_2 and measured mitochondrial DNA damage by qPCR analysis immediately after treatment and after 1, 2 or 4 hours of recovery. As shown in Figure 7A, *pif1*−/− MEFs showed a decreased capacity to repair stress-induced mtDNA lesions compared to control MEFs with an absence of recovery four hours after H_2O_2 treatment. The mtDNA damage phenotype was also confirmed by direct assessment of double strand breaks using one dimensional intact mtDNA agarose gel electrophoresis (1D-IMAGE) (Supplementary figure 2) (Kolesar et al., 2014). To demonstrate that depletion of PIF1 mitochondrial isoform (mPIF1^{67}) was responsible for the observed mtDNA repair deficiency in *pif1*−/− MEFs, we transduced both *pif1*+/+ (control) and *pif1*−/− MEFs with retrovirus

encoding the mitochondrial isoform. The transduction of *pif1*−/− MEFs resulted in significantly improved mtDNA repair capacity four hours after H_2O_2 treatment whereas transduction of control cells has no effect (Fig. 7A).

Mitochondrial DNA copy number was not different between control and *mPif1*−/− MEFs in basal conditions (not shown). We further explored the impact of H_2O_2 treatment on mtDNA level by qPCR during the recovery process. As previously described, we observed that ROS exposure did not immediately alter mtDNA content but the relative number of mtDNA molecules decreased during the process of recovery (Fig. 7B) (Rothfuss et al., 2010). Interestingly, mtDNA copy number decreased more rapidly in *pif1*−/− MEFs than in control cells suggesting that mtDNA was more severely damaged and degraded in PIF1-deficient cells (Fig. 7B). The $mPif1^{67}$ expression in *pif1*−/− MEFs led to a delay of mtDNA copy number decrease compared to mPif1-deficient cells after H_2O_2 treatment. All together, these results are consistent with a role of mPIF1 in mtDNA maintenance and repair after oxidative stress.

While mitochondria lack some repair pathways they have robust base excision repair of base damage resulting from oxidizing and alkylating agents (LeDoux et al., 1999; Sawyer and Van Houten, 1999). We asked whether PIF1 is also involved in mtDNA damage secondary to alkylating agents. We treated control and *pif1*−/− MEFs with methyl methanesulfonate (MMS). We observed that there was no delay to repair mtDNA lesions in KO MEFs compared to control MEFs after MMS treatment, suggesting that PIF1 is not involved in alkylation repair pathway (Fig. 7C).

4. DISCUSSION

Helicases are crucial enzymes in genome stability. While several mitochondrial helicases have been described, they remain poorly characterized (de Souza-Pinto et al., 2010; Ding and Liu, 2015). The mtDNA helicase encoded by the *TWINKLE* gene, also known as *PEO1,* is related to the phage T7 gp4 helicase-primase. TWINKLE, the first mammalian mitochondrial helicase identified, participates in mtDNA replication and has been shown to form a minimal mtDNA replisome *in vitro* together with the mitochondrial single-stranded DNA-binding protein and POLG, the sole mitochondrial DNA polymerase (Korhonen et al., 2004). Mutations in *TWINKLE* are mainly associated with autosomal dominant progressive external ophthalmoplegia (adPEO) (Copeland, 2008) but can also be responsible for severe recessive neurodegenerative disorder with CI deficiency (Hakonen et al., 2008). Mouse transgenic models that overexpressed several of the PEO mutations in *TWINKLE* (deletor mice) recapitulated many of the characteristics of human PEO, including late-onset mitochondrial myopathy and multiple mtDNA deletions (Tyynismaa et al., 2005). Human DNA2, a second member of the mitochondrial helicase family, was recently found in mammalian mitochondria where it participates in the removal of RNA primers during mtDNA replication due to its nuclease activity (Zheng et al., 2008). Human DNA2 interacts with POLG, stimulates its catalytic activity and most likely serves as an alternative to the TWINKLE helicase. Recently, mutations in *DNA2* have been identified in patients with adult-onset mitochondrial myopathy featuring instability of muscle mtDNA (Ronchi et al., 2013).

We show here that inactivation of *mPif1*, encoding another mitochondrial helicase, causes a mouse phenotype similar to those observed with *TWINKLE* and *DNA2* mutations. The mice developed a progressive mitochondrial myopathy. In muscle, we observed a mitochondrial accumulation in the subsarcolemmal region with abnormal mitochondria in animals at 14 months of age but no COX negative fibers. Interestingly, we also observed moth-eaten muscle fibers that have been described in association with CI defect and that correspond to necrotic fibers with a general disorganization of sarcomeres found by electron microscopy (Arenas et al., 1998). Another consequence of *PIF1* ablation is the complex I deficiency similar to that found in patients with infantile-onset spinocerebellar ataxia (IOSCA) carrying recessive *TWINKLE* mutations (Hakonen et al., 2008). Muscle weakness was confirmed by an impairment of exercise capacity particularly evident after one year of age. This decrease in physical activity is probably partly responsible for the weight gain observed in mice after 6 months of age. However, we can not exclude that the inactivation of *Pif1* causes metabolic abnormalities that should be investigated. In young *pif1*−/− animals, muscle morphology, biochemical analyses and physical performance revealed mild abnormalities suggesting that *Pif1* inactivation causes a slowly progressive disease; the mitochondrial defect becoming increasingly apparent under conditions of advanced age as with other mitochondriopathies. Despite Twinkle deletor mice and *pif1*−/− animals both develop a mitochondrial myopathy with mtDNA deletions, the phenotypic, biochemical and histological characteristics are quite different. Twinkle deletor mice show clear COX- fibers but yet their biochemistry is closed to normal. In contrast, *pif1*−/− animals show signs of exercise intolerance and muscle weakness with CI deficiency whereas Twinkle deletor mice don’t.

Here, we also show that PIF1 is involved in mtDNA maintenance. We found a low amount of mtDNA deletions in *pif1*−/− muscle. The number of deleted mtDNA molecules increased with age but was quite low after one year, resembling the findings in Twinkle deletor mice (Tyynismaa et al., 2005) and in some affected individuals harbouring *DNA2* or *TWINKLE* mutations (Ronchi et al., 2013; Suomalainen et al., 1997). It should also be noted that, as deletor mice, *pif1*−/− animals did not have an increased somatic mtDNA point mutation load in their muscle samples. Though the exact role of PIF1 helicase in mtDNA stability remains to be determined, it is likely that this protein is involved in the protection against oxidative damage. In yeast, *pif1*Δ mutants display elevated levels of oxidative mtDNA damage and mutagenesis (Doudican et al., 2005). The phenotypic severity of *pif1*Δ mutants may reflect the multifunctional role that ScPif1 mediates in response to mitochondrial oxidative stress, including inhibition of replication fork progression in order to allow time for repair to occur, controlling recombination, and other potential activities, such as influencing the accessibility of mtDNA to repair proteins (Doudican et al., 2005). The data presented here suggest that, in mammals, PIF1 is also involved in repair of oxidative damage in mitochondria because in response to H_2O_2 treatment, the recovery of mtDNA was delayed in *pif1*−/− MEFs compared to wild-type cells. Data revealing a shift in the relative abundance of circular and linear mtDNA in KO MEFs after H_2O_2 treatment is another argument in favor of this hypothesis. Furthermore, the number of mtDNA molecules decreased more rapidly during the recovery process in PIF1-deficient MEFs supporting the hypothesis that mtDNA recovery, involving replication of undamaged or repaired mtDNA molecules and degradation of affected mtDNA molecules, is more efficient in the presence of PIF1. Complementation

of PIF1-deficient MEFs with mPIF mitochondrial isoform had positive effects both on mtDNA repair capacity and amount of mtDNA molecules during the recovery process, thus demonstrating that the observed effects are specific to the PIF1 mitochondrial protein. Last, the induction of oxidative stress led to a significant increase of ROS level in *pif1*−/− MEFs compared to control cells. On the contrary, our results suggest that PIF1 is not involved in mtDNA repair generated by alkylating agents like MMS (Furda et al., 2012).

Oxidative lesions in the mitochondrial genome are repaired by base excision repair enzymes (BER). *In vitro* and *in vivo* experiments support a role for hDNA2 in mitochondrial long patch BER (LP-BER) with immunodepletion of hDNA2 from mitochondrial extracts resulting in decreased LP-BER activity (Zheng et al., 2008). *In vivo*, hDNA2 deficiency decreases repair of hydrogen peroxide-induced oxidative damage in mtDNA (Zheng et al., 2008) in the same way that the inactivation of *mPif1*. In yeast, it has been suggested that Pif1p generates long 5′ flaps which are removed by Dna2p (Budd et al., 2006). Since hDNA2 is largely mitochondrial, it is possible that in mammals these 2 proteins cooperate during mtDNA replication and/or repair, and the loss of these activities could lead to accumulation of intermediates that would, ultimately lead to mtDNA deletions. In the same way, TWINKLE is known as the mitochondrial replication helicase but it is not yet known whether it plays a role in mtDNA repair. However, the observed redistribution of mitochondrial DNA2 to the nucleoids in cells expressing mutated TWINKLE proteins (Duxin et al., 2009) also suggests a functional link between these mitochondrial helicases.

5. CONCLUSIONS

In conclusion, *Pif1* inactivation does not lead to dysfunctional telomeres in mouse but we show that animals develop a mitochondrial myopathy. *Pif1* inactivation is also responsible for a deficiency to repair oxidative stress-induced mtDNA damage. Improvement of mtDNA repair by complementation with the $PIF1^{67}$ mitochondrial-targeted form suggests that the mitochondrial phenotype observed in KO animals is due to the loss of the mPIF1 mitochondrial isoform. The similarity of human and mouse phenotypes associated with defects in TWINKLE, DNA2 or PIF1 is an additional argument in favor of the hypothesis of a functional interaction of these three helicases in the maintenance of mtDNA stability. These results open new perspectives for the study of mitochondrial helicases and for the exploration of patients with mtDNA instability disorders.

Supplementary Material

Refer to Web version on PubMed Central for supplementary material.

Acknowledgments

We thank Charlotte Cochaud and Sandra Foustoul for technical help. We thank the Animal Facility of IRCAN and the Pasteur-IRCAN Cellular and Molecular Imaging platform (PICMI). V.P-F was supported by the Fondation pour la Recherche Médicale (FRM - DPM20121125552) and the Association Française contre les Myopathies (AFM-16248); BAK and FRB were supported by NIH grant R01GM110424.

ABBREVIATIONS

COX	cytochrome *c* oxydase
SDH	succinate dehydrogenase
NADH-TR	nicotinamide adenine dinucleotide dehydrogenase tetrazolium reductase
mtDNA	mitochondrial DNA
OXPHOS	oxidative phosphorylation
LX-PCR	long extension-PCR
mPIF^{67}	mitochondrial PIF1 isoform
MEF	mouse embryonic fibroblast
MMS	methyl methanesulfonate
mtDIP-PCR	mtDNA immunoprecipitation PCR
KO	Knock-out
dATI	downstream alternative translation initiation
TBHP	Tert-nutyl hydroperoxide
NAC	N-acetylcysteine
ROS	reactive oxygen species
PEO	progressive external ophtalmoplegia
CI	complex I
GAPDH	glyceraldehyde 3-phosphate dehydrogenase
qPCR	quantitative polymerase chain reaction
nDNA	nuclear DNA

References

Arenas J, Campos Y, Ribacoba R, Martín MA, Rubio JC, Ablanedo P, et al. Complex I defect in muscle from patients with Huntington's disease. Ann Neurol. 1998; 43:397–400. [PubMed: 9506560]

Bannwarth S, Figueroa A, Fragaki K, Destroismaisons L, Lacas-Gervais S, Lespinasse F, et al. The human MSH5 (MutSHomolog 5) protein localizes to mitochondria and protects the mitochondrial genome from oxidative damage. Mitochondrion. 2012; 12:654–665. [PubMed: 22917773]

Bannwarth S, Procaccio V, Paquis-Flucklinger V. Surveyor™ nuclease: a new strategy for a rapid identification of heteroplasmic mitochondrial DNA mutations in patients with respiratory chain defects. Hum. Mutat. 2005; 25:575–582.

Bochman ML, Sabouri N, Zakian VA. Unwinding the functions of the Pif1 family helicases. DNA Repair. 2010; 9:237–249. [PubMed: 20097624]

Bradford MM. A rapid and sensitive method for the quantitation of microgram quantities of protein utilizig the principle of protein-dye binding. Anal Biochem. 1976; 72:248–254. [PubMed: 942051]

Budd ME, Reis CC, Smith S, Myung K, Campbell JL. Evidence suggesting that Pif1 helicase functions in DNA replication with the Dna2 helicase/nuclease and DNA polymerase delta. Mol Cell Biol. 2006; 26:2490–2500. [PubMed: 16537895]

Copeland WC. Inherited mitochondrial diseases of DNA replication. Ann Rev Med. 2008; 59:131–146. [PubMed: 17892433]

De Bono JP, Adlam D, Paterson DJ, Channon KM. Novel quantitative phenotypes of exercise training in mouse models. Am J Physiol Regul Integr Comp Physiol. 2006; 290:R926–934. [PubMed: 16339385]

de Souza-Pinto NC, Aamann MD, Kulikowicz T, Stevnsner TV, Bohr VA. Mitochondrial helicases and mitochondrial genome maintenance. Mech Ageing Dev. 2010; 131:503–510. [PubMed: 20576512]

Ding L, Liu Y. Borrowing nuclear DNA helicases to protect mitochondrial DNA. Int J Mol Sci. 2015; 16:10870–10887. [PubMed: 25984607]

Doudican NA, Song B, Shadel GS, Doetsch PW. Oxidative DNA damage causes mitochondrial genomic instability in Saccharomyces cerevisiae. Mol Cell Biol. 2005; 25:5196–5204. [PubMed: 15923634]

Duxin JP, Dao B, Martinsson P, Rajala N, Guittat L, Campbell JL, et al. Human Dna2 is a nuclear and mitochondrial DNA maintenance protein. Mol Cell Biol. 2009; 29:4274–4282. [PubMed: 19487465]

Edgar D, Shabalina I, Camara Y, Wredenberg A, Calvaruso MA, Nijtmans L, et al. Random point mutations with major effects on protein-coding genes are the driving force behind premature aging in mtDNA mutator mice. Cell Metab. 2009; 10:131–138. [PubMed: 19656491]

Foury F, Kolodynski J. pif mutation blocks recombination between mitochondrial rho+ and rho− genomes having tandemly arrayed repeat units in Saccharomyces cerevisiae. Proc Natl Acad Sci U S A. 1983; 80:5345–5349. [PubMed: 6310571]

Furda A, Marrangoni A, Lokshin A, Van Houten B. Oxidants and not alkylating agents induce rapide mtDNA loss and mitochondrial dysfunction. DNA Repair. 2012; 11:684–692. [PubMed: 22766155]

Futami K, Shimamoto A, Furuichi Y. Mitochondrial and nuclear localization of human Pif1 helicase. Biol Pharm Bull. 2007; 30:1685–1692. [PubMed: 17827721]

George T, Wen Q, Griffiths R, Ganesh A, Meuth M, Sanders CM. Human Pif1 helicase unwinds synthetic DNA structures resembling stalled DNA replication forks. Nucleic Acids Res. 2009; 37:6491–6502. [PubMed: 19700773]

Hakonen AH, Goffart S, Marjavaara S, Paetau A, Cooper H, Mattila K, et al. Infantile-onset spinocerebellar ataxia and mitochondrial recessive ataxia syndrome are associated with neuronal complex I defect and mtDNA depletion. Hum Mol Genet. 2008; 17:3822–3835. [PubMed: 18775955]

Kazak L, Reyes A, Duncan AL, Rorbach J, Wood SR, Brea-Calvo G, et al. Alternative translation initiation augments the human mitochondrial proteome. Nucleic Acids Res. 2013; 41:2354–2369. [PubMed: 23275553]

Kolesar JE, Safdar A, Abadi A, MacNeil LG, Crane JD, Tarnopolsky MA, et al. Defects in mitochondrial DNA replication and oxidative damage in muscle of mtDNA mutator mice. Free Radic Biol Med. 2014; 75:241–251. [PubMed: 25106705]

Kolesar JE, Wang CY, Taguchi YV, Chou SH, Kaufman BA. Two-dimensional intact mitochondrial DNA agarose electrophoresis reveals the structural complexity of the mammalian mitochondrial genome. Nucleic Acids Res. 2013; 41:e58. [PubMed: 23275548]

Korhonen JA, Pham XH, Pellegrini M, Falkenberg M. Reconstitution of a minimal mtDNA replisome in vitro. EMBO J. 2004; 23:2423–2429. [PubMed: 15167897]

Lahaye A, Leterme S, Foury F. PIF1 DNA helicase from Saccharomyces cerevisiae. Biochemical characterization of the enzyme. J Biol Chem. 1993; 268:26155–26161. [PubMed: 8253734]

LeDoux SP, Driggers WJ, Hollensworth BS, Wilson GL. Repair of alkylation and oxidative damage in mitochondrial DNA. Mutat Res. 1999; 434:149–159. [PubMed: 10486589]

Li JR, Yu TY, Chien IC, Lu CY, Lin JJ, Li HW. Pif1 regulates telomere length by preferentially removing telomerase from long telomere ends. Nucleic Acids Res. 2014; 42:8527–8536. [PubMed: 24981509]

Morales CP, Holt SE, Ouellette M, Kaur KJ, Yan Y, Wilson KS, et al. Absence of cancer-associated changes in human fibroblasts immortalized with telomerase. Nat Genet. 1999; 21:115–118. [PubMed: 9916803]

Neyton S, Lespinasse F, Moens PB, Paul R, Gaudray P. Association between MSH4 (MutS homolog 4) and the DNA strand-exchange RAD51 and DMC1 proteins during mammalian meiosis. Mol Hum Reprod. 2004; 10:917–924. [PubMed: 15489243]

Paeschke K, Bochman ML, Garcia PD, Cejka P, Friedman KL, Kowalczykowski SC, et al. Pif1 family helicases suppress genome instability at G-quadruplex motifs. Nature. 2013; 497:458–462. [PubMed: 23657261]

Ronchi D, Di Fonzo A, Lin W, Bordoni A, Liu C, Fassone E, et al. Mutations in DNA2 Link Progressive Myopathy to Mitochondrial DNA Instability. Am J Hum Genet. 2013; 92:293–300. [PubMed: 23352259]

Rothfuss O, Gasser T, Patenge N. Analysis of differential DNA damage in the mitochondrial genome employing a semi-long run real-time PCR approach. Nucleic Acids Res. 2010; 38:e24. [PubMed: 19966269]

Rouzier C, Bannwarth S, Chaussenot A, Chevrollier A, Verschueren A, Bonello-Palot N, et al. The MFN2 gene is responsible for mitochondrial DNA instability and optic atrophy ‘plus’ phenotype. Brain. 2012; 135:23–34. [PubMed: 22189565]

Rustin P, Chrétien D, Bourgeron T, Gérard B, Rotig A, Saudubray JM, et al. Biochemical and molecular investigations in respiratory chain deficiency. Clin Chim Acta. 1994; 228:35–51. [PubMed: 7955428]

Sahin E, Colla S, Liesa M, Moslehi J, Müller FL, Guo M, et al. Telomere dysfunction induces metabolic and mitochondrial compromise. Nature. 2011; 470:359–365. [PubMed: 21307849]

Sanders CM. Human Pif1 helicase is a G-quadruplex DNA-binding protein with G-quadruplex DNA-unwinding activity. Biochem J. 2010; 430:119–128. [PubMed: 20524933]

Sawyer DE, Van Houten B. Repair of DNA damage in mitochondria. Mutat Res. 1999; 434:161–176. [PubMed: 10486590]

Schulz VP, Zakian VA. The saccharomyces PIF1 DNA helicase inhibits telomere elongation and de novo telomere formation. Cell. 1994; 76:145–155. [PubMed: 8287473]

Shull S, Heintz NH, Periasamy M, Manohar M, Janssen YM, Marsh JP, et al. Differential regulation of antioxidant enzymes in response to oxidants. J Biol Chem. 1991; 266:24398–24403. [PubMed: 1761541]

Snow BE, Mateyak M, Paderova J, Wakeham A, Iorio C, Zakian VA, et al. Murin Pif1 interacts with telomerase ans is dispensable for telomere function in vivo. Mol Cell Biol. 2007; 27:1017–1026. [PubMed: 17130244]

Suomalainen A, Majander A, Wallin M, Setälä K, Kontula K, Leinonen H, et al. Autosomal dominant progressive external ophthalmoplegia with multiple deletions of mtDNA: clinical, biochemical, and molecular genetic features of the 10q-linked disease. Neurology. 1997; 48:1244–1253. [PubMed: 9153451]

Tyynismaa H, Mjosund KP, Wanrooij S, Lappalainen I, Ylikallio E, Jalanko A, et al. Mutant mitochondrial helicase Twinkle causes multiple mtDNA deletions and a late-onset mitochondrial disease in mice. Proc Natl Acad Sci USA. 2005; 102:17687–17692. [PubMed: 16301523]

Tyynismaa H, Sembongi H, Bokori-Brown M, Granycome C, Ashley N, Poulton J, et al. Twinkle helicase is essential for mtDNA maintenance and regulates mtDNA copy number. Hum Mol Genet. 2004; 13:3219–3227. [PubMed: 15509589]

Wilson MA, Kwon Y, Xu Y, Chung WH, Chi P, Niu H, et al. Pif1 helicase and Pold promote recombination-coupled DNA synthesis via bubble migration. Nature. 2013; 502:393–396. [PubMed: 24025768]

Yakes FM, Van Houten B. Mitochondrial DNA damage is more extensive and persists longer than nuclear DNA damage in human cells following oxidative stress. Proc Natl Acad Sci USA. 1997; 94:514–519. [PubMed: 9012815]

Zhang DH, Zhou B, Huang Y, Xu LX, Zhou JQ. The human Pif1 helicase, a potential Escherichia coli RecD homologue, inhibits telomerase activity. Nucleic Acids Res. 2006; 34:1393–1404. [PubMed: 16522649]

Zheng L, Zhou M, Guo Z, Lu H, Qian L, Dai H, et al. Human DNA2 is a mitochondrial nuclease/helicase for efficient processing of DNA replication and repair intermediates. Mol Cell. 2008; 32:325–336. [PubMed: 18995831]

Zhou J, Monson EK, Teng SC, Schulz VP, Zakian VA. Pif1p helicase, a catalytic inhibitor of telomerase in yeast. Science. 2000; 289:771–774. [PubMed: 10926538]

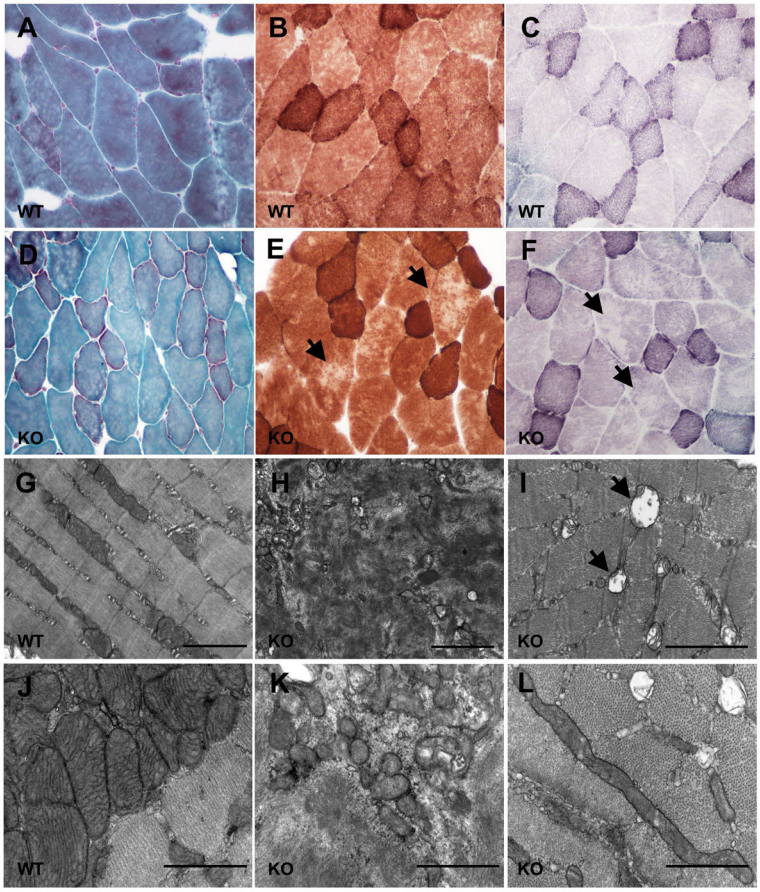

Figure 1. Muscle analysis from 14-month-old control and *pif1*−/− mice

A–F. Histopathology of control (A–C) and KO (D–F) mice with Gomori modified trichrome (A, D) showing an accumulation of mitochondria in the subsarcolemmal region in *pif1*−/− mice, COX/SDH (B, E) and NADH-TR (C, F) staining revealing moth-eaten fibers in the same animals (arrows). **G–L.** Ultrastructure of skeletal muscle from control (G, J) and KO (H, I, K, L) mice showing some necrotic fibers characterized by an erasing of the striation and a general disorganization of sarcomeres (H, K) and mitochondrial abnormalities such as emphasis of mitochondria contours and lost of cristae (K). Other fibers show enlarged and swollen mitochondria with altered cristae organization (I, arrows) or elongated mitochondria (L) in *pif1*−/− mice. Scale bars: G, H, I: 2 μm, J, K, L: 1 μm.

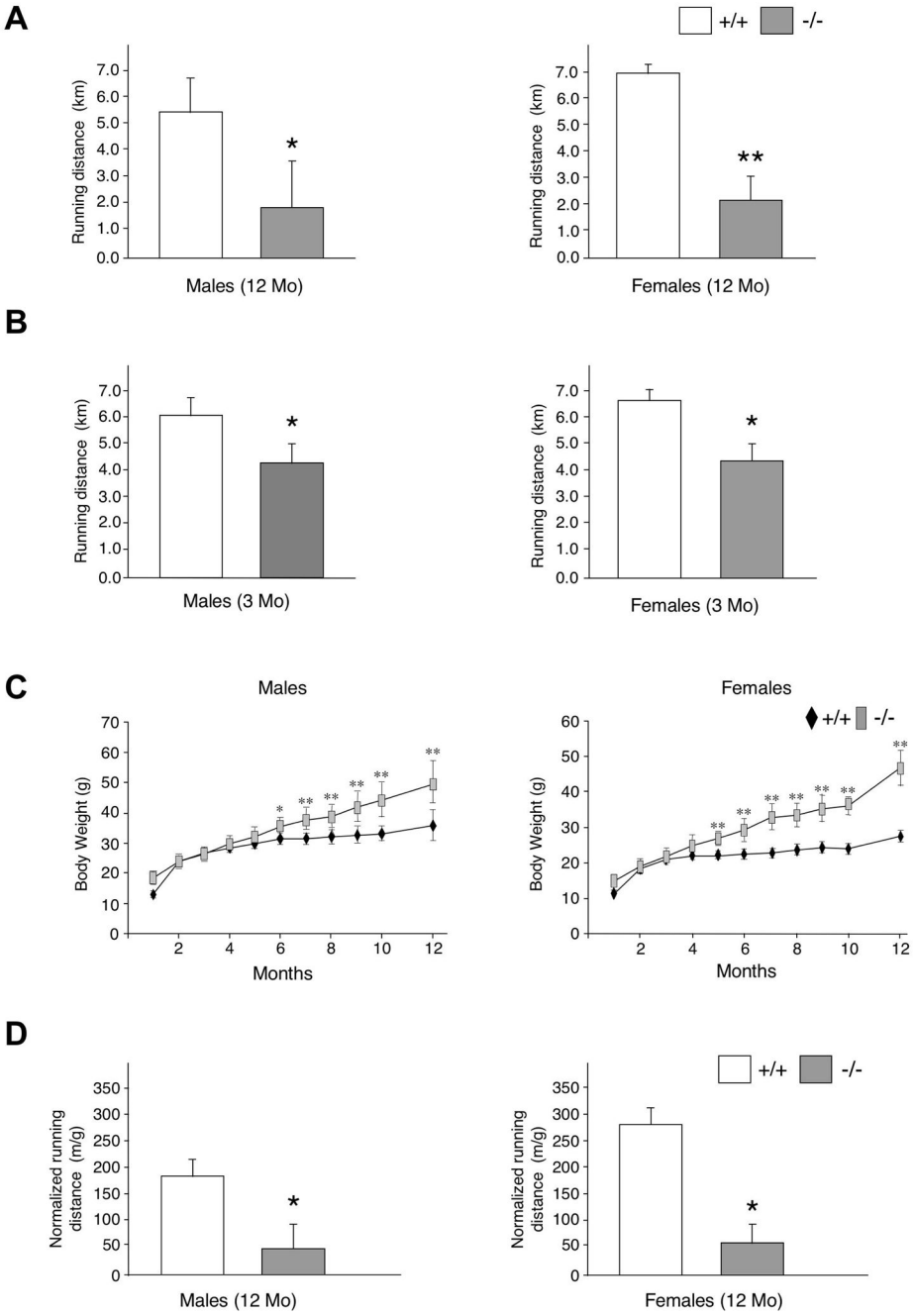

Figure 2. Physical performance of control and *pif1*−/− mice

A. Average distance run voluntarily per day by males (left panel, n=6) and females (right panel, n=6) at 12 months of age. **B.** Average distance run voluntarily per day by males (left panel, n=6) and females (right panel, n=6) at 3 months of age. **C.** Left panel: body weight curves for male wild-type (n=9 at the different time points, black diamonds) and *pif1*−/− (n=6–11, grey rectangles) mice. Right panel: body weight curves for female wild-type (n=4–7, black diamonds) and *pif1*−/− (n=4–11, grey rectangles) mice. **D.** Body weight-normalized running distance from males (left panel) and females (right panel) at 12 months of age. Mo:

month; km: kilometer; m/g: meter/gram; +/+: wild-type and −/−: KO mice. Differences were analyzed by the Student's *t* test (*: P<0.05; **: P<0.01).

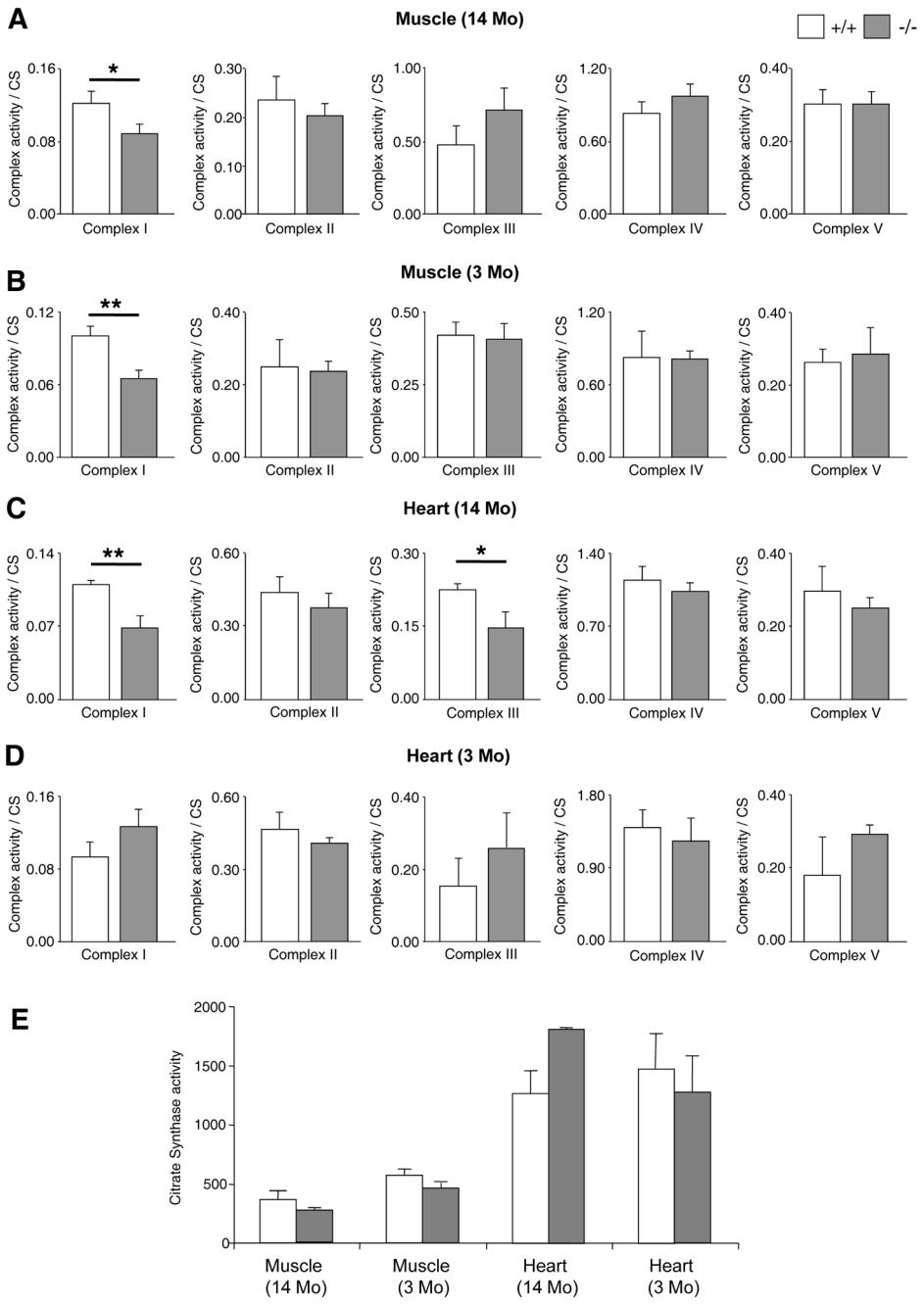

Figure 3. Spectrophotometric analysis of respiratory chain in wild-type and *pif1*−/− mice

A. Muscle from mice at 14 months (Mo) of age. **B.** Muscle from mice at 3 months of age. **C.** Heart from mice at 14 months of age. **D.** Heart from mice at 3 months of age. Results represent the mean ± SD of 3 independent experiments from 3 wild-type and 3 *pif1*−/− mice. Activities were expressed as activity ratios compared to citrate synthase (CS). **E.** Citrate synthase activity in A, B, C and D samples. Differences in respiratory complex activities were analyzed by the Student's *t* test (*: P<0.05; **: P<0.01).

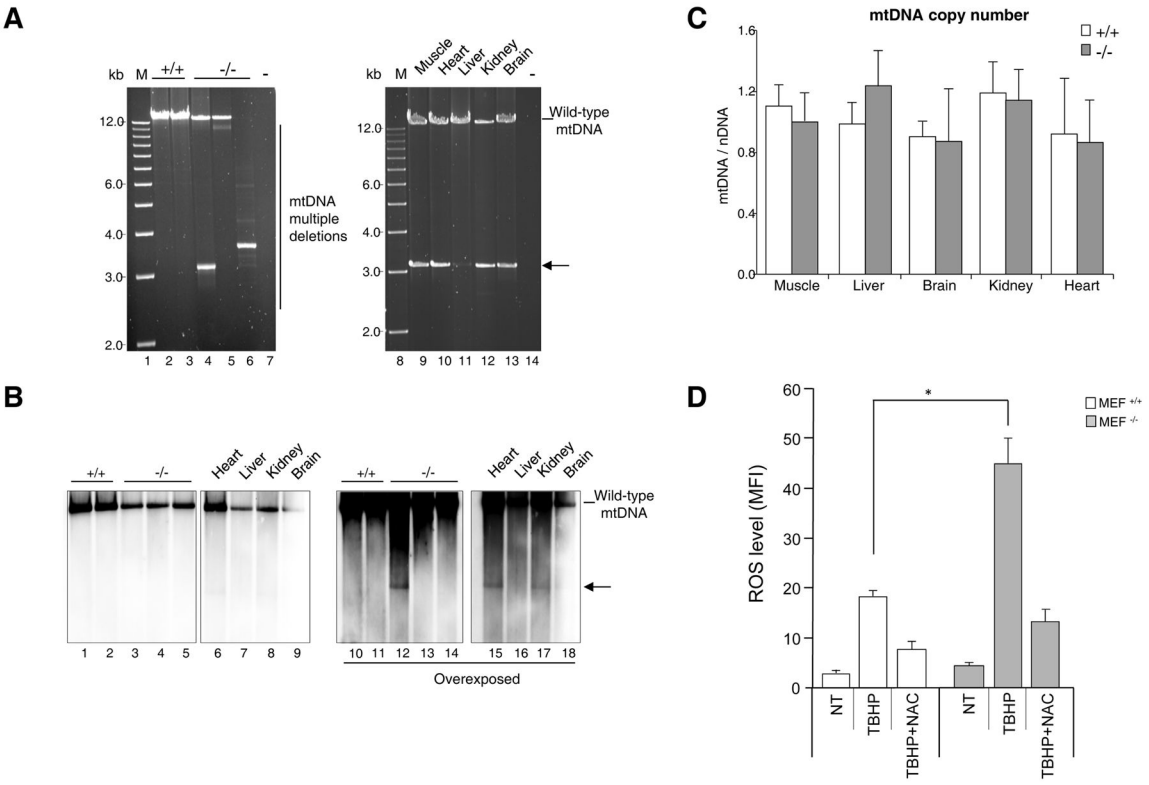

Figure 4. Mitochondrial DNA analysis and copy number determination

A. Long extension PCR of mtDNA from muscle of 2 wild-type (lanes 2, 3) or 3 *pif1*−/− (lanes 4–6) mice at 14 months of age and from muscle, heart, liver, kidney and brain (lanes 9–13) of the *pif1*−/− mouse corresponding to lane 4. Arrow indicates the 3kb amplicon. Lanes 1, 8: molecular weight marker; 1kb Plus DNA Ladder (Life Technologies). Lanes 7, 14: negative PCR controls. **B.** Southern blot of muscles (lanes 1–5 and 10–14) and other tissues (lanes 6–9 and 15–18) of 14-month-old wild-type (lanes 1, 2, 10, 11) and *pif1* −/− (lanes 3–9 and 12–18) mice. The right panel corresponds to the overexposed version of the Southern blot showed on the left panel. The deleted molecule corresponding to the 3kb amplicon is pointed by the arrow. **C.** Determination of mtDNA content. Mitochondrial DNA quantification in muscle, liver, brain, kidney and heart of wild-type (white) or *pif1*−/− (grey) mice at the age of 14 months. The mouse mitochondrial 12S rRNA (mtDNA) and the nuclear GAPDH (nDNA) genes were individually amplified by real-time PCR. Data were expressed as *ratio* between mtDNA and nDNA concentration and values were normalized to wild-type sample. Results represent the mean of relative PCR ± SD of 3 independent experiments from 3 wild-type and 3 *pif1*−/− mice. **D.** ROS level production in MEFs by flow cytometry. Wild-type (white) and *pif1*−/− (grey) MEFs were pretreated with 500μM or without antioxydant NAC for one hour. Cells were then incubated with 200μM TBHP (ROS inducer) and stained with CellROX green reagent. Results represent the mean of two independent experiments ± SEM. Differences were analyzed by Student's *t* test (*: $p<0.05$). MFI: median fluorescence intensity, NT: not treated cells.

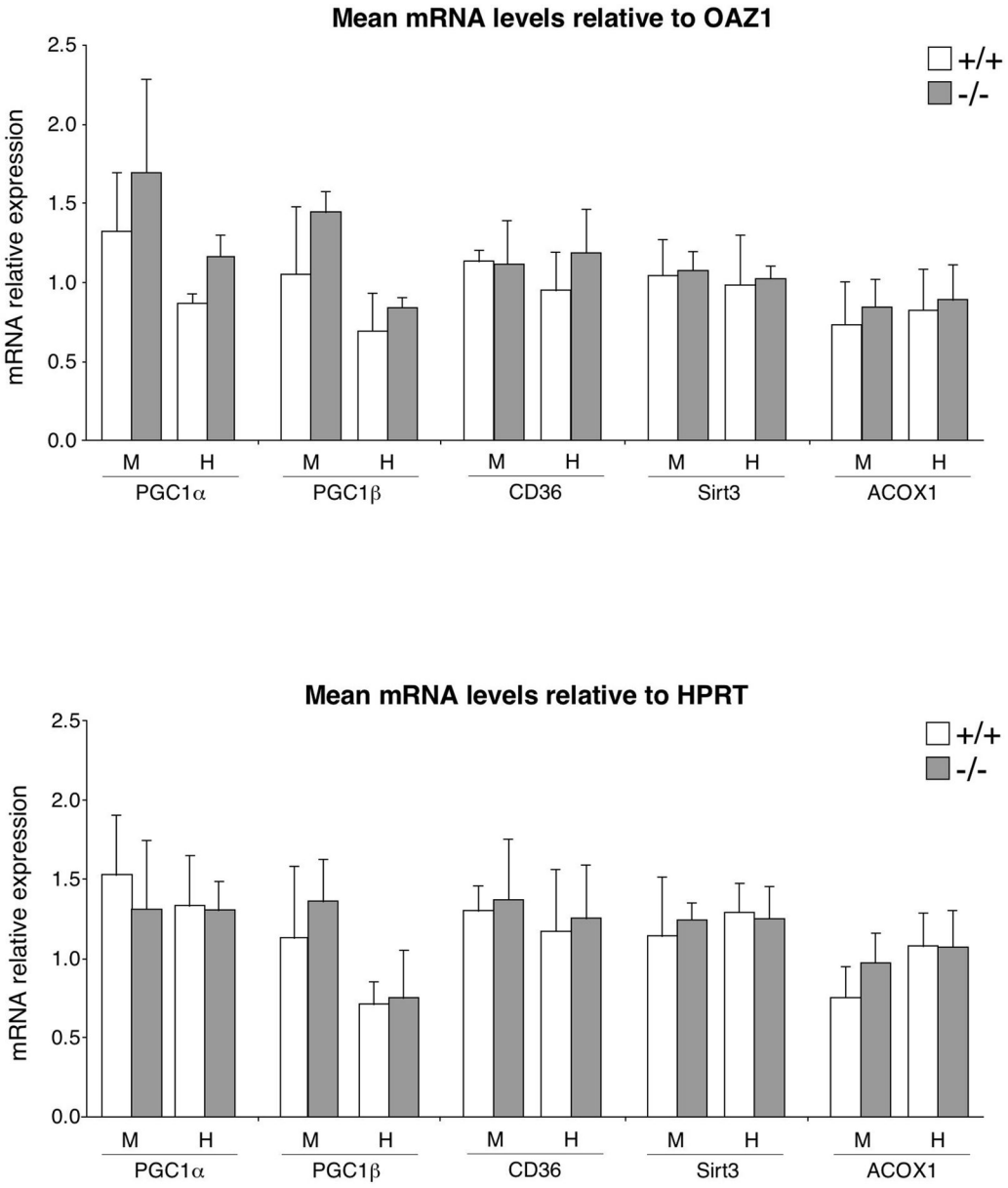

Figure 5. Quantitative Real-Time PCR analysis of PGC pathway in wild-type and *pif1−/−* mice

RT-qPCR analysis of *PGC-1α*, *PGC-1β* and transcriptional targets (*Sirt3*, *CD36, Acox1*) in muscle (M) and in heart (H) of control (white) and *Pif1−/−* (grey) 14-month-old mice. Results were normalized to *OAZ1* (upper panel) and *HPRT* (lower panel). Results represent the mean of relative PCR ± SD of 3 independent experiments from 3 wild-type and 3 *pif1−/−* mice.

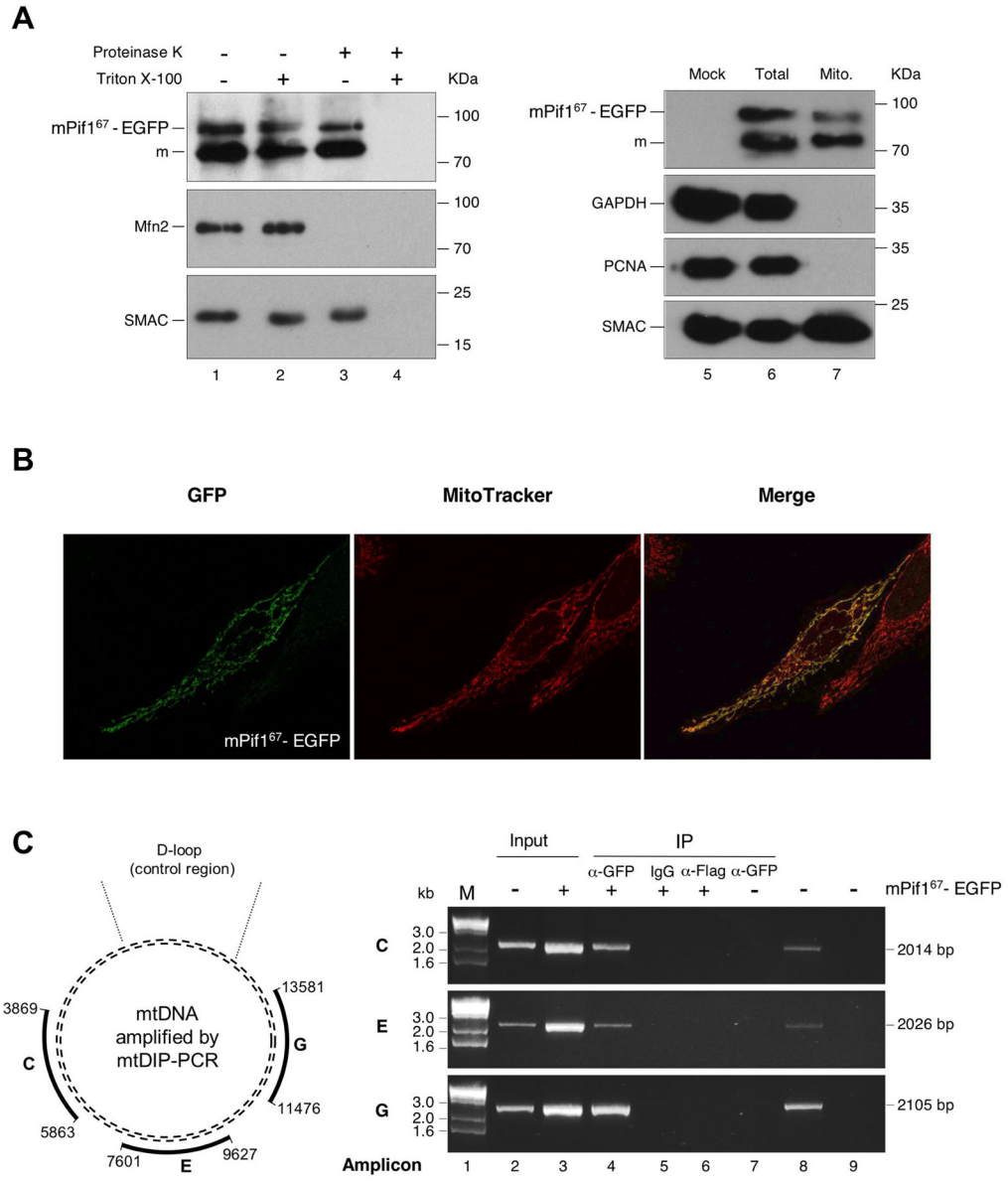

Figure 6. Mitochondrial localization of PIF1 and association with mtDNA

A. Intact isolated mitochondria (lanes 1–4, 7) from mPif1^{67}-EGFP transfected HeLa cells were incubated in presence (+) or in absence (−) of Proteinase K or Triton X-100 before analysis by immunoblotting using antibodies against GFP, MFN2 (mitochondrial outer membrane protein) or SMAC (mitochondrial intermembrane space protein). To verify the purity of isolated mitochondria, total lysates of untransfected cells (lane 5), *mPIF1^{67}-EGFP* transfected cells (lane 6) and mitochondrial isolates (lane 7) were analyzed by immunoblotting using antibodies against GAPDH (cytosolic protein), PCNA (nuclear protein) or SMAC (mitochondrial protein). m: putative mature dATI isoform of mPIF1^{67} after mitochondrial import and removal of the MTS (Mitochondrial Targeting Sequence). **B.** Confocal microscopy images of *mPIF1^{67}-EGFP* transfected HeLa cells stained with MitoTracker. **C.** mtDIP-PCR analysis of mPIF1^{67}-EGFP binding *in vivo*. Left panel:

Schematic diagram of the mitochondrial genome (dotted line). The regions of the mtDNA which were amplified by PCR are represented with primer positions (thick line). Numbers correspond to mtDNA nucleotides (GenBank NC_012920). Right panel: Agarose gel of PCR products for amplicons C, E or G containing either mtDNA co-immunoprecipitated (IP) with anti-GFP (lanes 4, 7), IgG (lanes 5) or anti-Flag (lanes 6). Input: PCR positive control (mtDNA before immunoprecipitation). M: molecular weight marker 1kb Plus (Life Technologies). Lanes 8: PCR positive control. Lanes 9: “no template” PCR negative control.

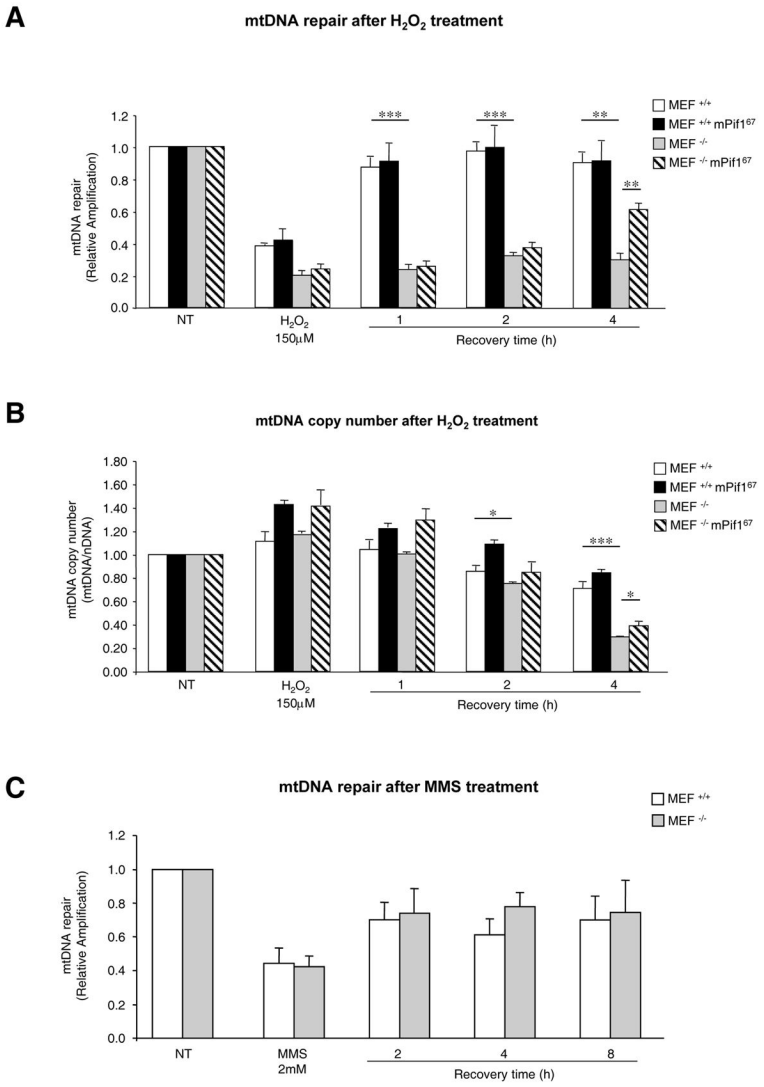

Figure 7. mtDNA repair following DNA damage induced by oxidative or alkylating stress in MEFs and complementation with the mitochondrial isoform

A. mtDNA repair activity after H_2O_2-induced DNA damage in wild-type (white), wild-type + *mPIF1*^{67} (black), *pif1*−/− (grey) and *pif1*−/− + *mPIF1*^{67} (hatched) MEFs. A long-range PCR was used to evaluate the oxidative damage, induced by H_2O_2 treatment, in mtDNA. The relative PCR amplification of a 15.6kb mtDNA fragment was normalized to mtDNA copy number that was evaluated by PCR amplification of a 172bp mtDNA fragment. **B.** Determination of the mtDNA copy number after H_2O_2 treatment. mtDNA/nDNA values in wild-type (white), wild-type + *mPIF1*^{67} (black), *pif1*−/− (grey) and *pif1*−/− + *mPIF1*^{67} (hatched) MEFs. mtDNA: mitochondrial DNA, nDNA: nuclear DNA. A–B. Cells were exposed to 150µM H_2O_2 for 30 min and either harvested immediately or allowed to recover in conditioned medium for the indicated times. **C.** mtDNA repair activity after MMS-induced DNA damage in wild-type (white) and *pif1*−/− (grey) MEFs. A long-range PCR was used to evaluate the alkylating damage induced by MMS treatment. The relative PCR amplification of a 15.6kb mtDNA fragment was normalized to mtDNA copy number that

was evaluated by PCR amplification of a 172bp mtDNA fragment. Results represent the mean of relative PCR amplification ± SEM of two independent experiments in which three PCRs per point were performed. Values were normalized to untreated cells and differences were analyzed by Student's *t* test (*: $p<0.05$, **: $P<0.01$).